REPORT DOCUMENTATION PAGE

AFRL-SR-AR-TR-07-0013

1. REPORT DATE *(DD-MM-YYYY)*	2. REPORT TYPE	3. DATES COVERED *(From - To)*
	FINAL REPORT	15 AUG 2003 - 14 SEP 2006

4. TITLE AND SUBTITLE
(HBCU/MI) COUPLED QUANTUM DOTS AND PHOTONIC CRYSTALS FOR NANOPHOTONIC DEVICES

5a. CONTRACT NUMBER

5b. GRANT NUMBER
F49620-03-1-0433

5c. PROGRAM ELEMENT NUMBER
61102F

6. AUTHOR(S)
PROFESSOR HUFFAKER

5d. PROJECT NUMBER
4113/HX

5e. TASK NUMBER

5f. WORK UNIT NUMBER

7. PERFORMING ORGANIZATION NAME(S) AND ADDRESS(ES)
UNIVERSITY OF NEW MEXICO
SCHOLES HALL ROM 102
ALBUQUERQUE NM 87131-0001

8. PERFORMING ORGANIZATION REPORT NUMBER

9. SPONSORING/MONITORING AGENCY NAME(S) AND ADDRESS(ES)
AF OFFICE OF SCIENTIFIC RESEARCH
875 N RANDOLPH STREET RM 3112
ARLINGTON VA 22203
PROGRAM MANAGER: GERNOT POMRENKE/NE

10. SPONSOR/MONITOR'S ACRONYM(S)

11. SPONSOR/MONITOR'S REPORT NUMBER(S)

12. DISTRIBUTION/AVAILABILITY STATEMENT
DISTRIBUTION STATEMENT A: UNLIMITED

13. SUPPLEMENTARY NOTES

14. ABSTRACT
To this end we worked to combine engineered QD5 with engineered PC cavities to explore and exploit simultaneous electronic and optical confinement. Technical thrusts included Nanocavity design and device development along with integration with the quantum dot active (QD) region. The first approach which we considered was to incorporate self-assembled QD5 into the starting epitaxial material, where the PC nanocavities are fabricated after growth. The PCs design and fabrication was optimized for high cavity Q and minimal cavity volume. In parallel, we developed nanopatterning capability to arbitrarily place a single QD or an ensemble of identical QUs within the PC.

15. SUBJECT TERMS
THRUSTS

16. SECURITY CLASSIFICATION OF:			17. LIMITATION OF ABSTRACT	18. NUMBER OF PAGES	19a. NAME OF RESPONSIBLE PERSON
a. REPORT	b. ABSTRACT	c. THIS PAGE			19b. TELEPHONE NUMBER *(Include area code)*

Coupled Quantum Dots and Photonic Crystals for Nanophotonic Devices

Principal Investigator and Technical Point of Contact:
Associate Professor, Diana L. Huffaker
Center for High Technology Materials,
Department of Electrical Engineering,
University of New Mexico, 1313 Goddard SE, Albuquerque 87106
Voice: 505 272 7845 FAX: 505 272 7801 e-mail: huffaker@chtm.unm.edu

Co-Principal Investigator:
Professor Kent D. Choquette
Micro and Nanotechnology Laboratory,
Department of Electrical and Computer Engineering,
University of Illinois at Urbana-Champaign,
208 North Wright Street, Urbana, IL 61801
Voice: 217 265 0563 FAX: 217 244 6375 e-mail: choquett@uiuc.edu

FINAL REPORT

SUBMITTED TO DR. GERNOT POMRENKE, AFRL/AFOSR

by
University of New Mexico, Albuquerque

Table of Contents

I. Program Objective: *Develop nanophotonic devices based upon coupled QD emitters in a PhC nanocavity.*

The ultimate objective of the proposed research was to establish the next generation of nano-photonic light sources and optical memory. To this end we worked to combine engineered QDs with engineered PC cavities to explore and exploit simultaneous electronic and optical confinement. Technical thrusts included Nanocavity design and device development along with integration with the quantum dot active (QD) region. The first approach which we considered was to incorporate self-assembled QDs into the starting epitaxial material, where the PC nanocavities are fabricated after growth. The PCs design and fabrication was optimized for high cavity Q and minimal cavity volume. In parallel, we developed nanopatterning capability to arbitrarily place a single QD or an ensemble of identical QDs within the PC. The outcome of these thrust areas are described below.

II. Technical Thrusts:

a. Quantum Dot Nano-Cavity Development:

Fabricate 2D nanocavity devices with self-assembled and nanopatterned QD active regions.

The nanocavity devices samples are grown by metal organic chemical vapor deposition (MOCVD) at 60 Torr using trimethylgallium (TMGa), trimethylindium (TMIn), tertiarybutylphoshine (TBP) and Arsine (AsH3) or tertiarybuthyarsine (TBA). Two types of structures have been grown, optically and electrically injected structures. The cross-sectional of the diode structures are shown in figure 1. In this structure, growth is initiated on a GaAs (001) substrate with a 3000 Å GaAs layer at 680 °C after the thermal deoxidation step at 820 °C. Next, at same growth temperature, 1000 nm of undoped $Al_{0.94}Ga_{0.06}As$ layer was grown. Then the temperature is reduced and stabilized for active region growth within the range of 450-520 °C. The active region consist of a 5 ML $In_{0.15}Ga_{0.85}As$ buffer layer, a 3 ML InAs QD coverage, and a 25 ML $In_{0.15}Ga_{0.85}As$ cap. A post nucleation AsH_3 pause is used after the growth of each QD layer to reduce the defect density. The stacked QD layers are separated by a GaAs barrier sandwiching the GaP strain-compensation layer. The strain compensation layers were use to compensated the compressive strain in active region, which results in lower defect density and improved PL efficiency. The optimization of GaP thickness is 4 MLs, results in 36 % of strain reduction in our structure. The SC layer thickness are measured from high resolution transmission electron microscopy (TEM) images and confirm by high resolution x-ray diffraction (HRXRD). The interface regions, GaAs/GaP and GaP/GaAs, are optimized through the switching of gas flows to minimize In segregation and As-P interchange. The total thickness of SAQD active region was fixed at 220 nm.

Room temperature photoluminescence (RTPL) from a series of optically pumped nanocavity device samples with varied number of stacking including 1, 6 and 10 stacks was also studied. Several trends can be observed here. Overall, the PL intensity of 6 stacks and 10 stacks samples are more than one order of magnitude higher with GaP SC layers than without. As the staking number increases from 1 stack to 6 stacks, we observe a red shift from 1.30 μm to 1.31 μm due to increased in QD size driven by the accumulated strain. The PL intensity increases with stacking number from 1 stack to 6 stacks then decreases for 10 stacks. The decrease in PL intensity associated with

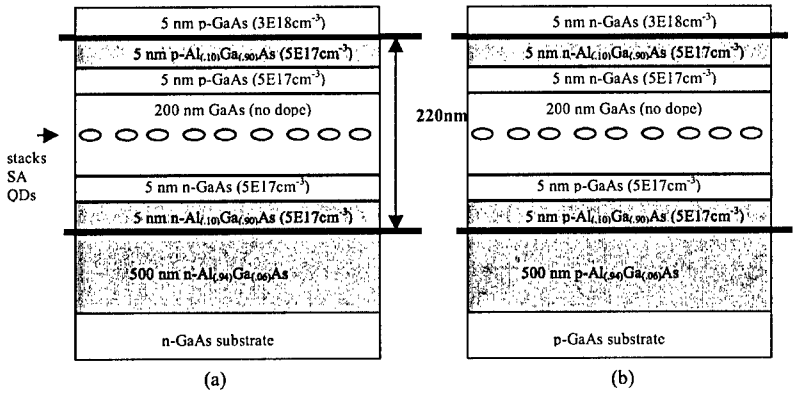

Figure 1 Schematic illustration of electrically pumped structure containing stacked InAs SAQD. (a) p side-up and (b)n side-up structures.

the number of stacking can be attributed to increased defect density in the structure as result of high accumulated strain. This result suggest that number of stacking for nanocavity devices should not be more than 6 stacks.

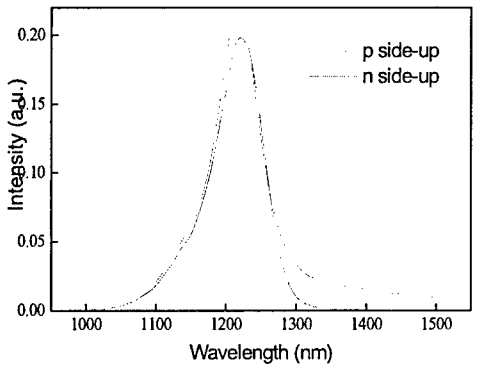

Figure 2 RTEL of electrically pumped structures.

The cross-sectional of electrically pumped structures are schematically illustrated in figure 2 (a) p side-up structure and (b) n side-up structure. In the p side-up structure (a), Si-doped (with density of 5×10^{18} cm^{-3}) n-type GaAs substrate has been used. After the thermal deoxidation step at 820 °C, 300 nm of n-doped GaAs (with doping density of 5×10^{18} cm^{-3}), using silicon for dopant, was grown at 720 °C. Next, at same growth temperature, 500 nm of n-doped (doping density of 2×10^{18} cm^{-3}) $Al_{0.94}Ga_{0.06}As$ layer were grown followed by 5 nm of n-doped (doping density of 5×10^{17} cm^{-3}) $Al_{0.10}Ga_{0.90}As$ lower clad layer (LCL) and 5 nm n-GaAs at the same doping level. Then, the temperature of the substrate was decreased to 520 °C, and strain-compensated SAQD stacks were formed using the growth parameters close to those in optically pumped structure. Then, the active regions were capped by 5 nm of C-doped (doping density of 5×10^{17} cm^{-3}) GaAs followed by a 5m p-doped$Al_{0.10}Ga_{0.90}As$ lower clad layer (UCL) at the same doping level with increasing the substrate temperature from 520 °C to 560 °C. At the final growth step, p+-doped (doping density of 3×10^{18} cm^{-3}) GaAs contact layer was grown. For n side-up structure (b), both growth procedures and growth parameters are similar to p side-up structure but with the opposite p-doped and n-doped layers. It should be noted here that highly p-doped (doping density of 2×10^{18} cm^{-3}) $Al_{0.94}Ga_{0.06}As$ layer in figure 3 (b) was not achieved by C-doping, but by Zn-doping. The RTPL spectra of the electrically pumped structure is shown in figure 4. The result shows very similar emitting wavelength and FWHM in both structures, suggesting no different in SAQD formation between these two structures.

b.) Design, fabricate, characterize opto-electronic devices (LEDs, lasers).

Photonic Crystal Design

In order to design the photonic crystal defect nanocavity, first we have to calculate the photonic band structure using the plane wave method [1]. The spectra and quality of the defect mode in the cavity can be determined from the time evolution of the resonant mode propagation calculated using the finite-difference time-domain (FDTD) method [2], which will be discussed later. In general, there are three design parameters: the thickness of the semiconductor membrane (t), the lattice spacing (a), and the radius (r) of the air hole in the photonic crystal. The generated modes from the photonic crystal with infinite thickness (air holes) are classified as transverse electric (TE) and transverse magnetic (TM) modes in Figure 3. TE modes are defined as the electric field polarized normal to the axis of air holes, and TM modes as the electric field polarized parallel to the axis of air holes [3]. The modes are thus classified as TE and TM modes, but they can also have even and odd spatial symmetry with respect to the center of the slab. However, the resonant modes of the 2-D photonic crystal slab with finite thickness are not purely TE or TM, rather they are designated as TE-like and TM-like modes [4]. The TE-like and TM-like modes are classified by a horizontal mirror operation in the middle of the slab. TE-like modes are even under mirror reflection, while the TM-like modes are odd. Thus, TE-like modes consist of even TE slab modes and odd TM modes. The quantum wells in the slab are designed to provide gain for electric fields polarized in the plane of the quantum wells, which are TE slab modes. Therefore, our designs are focused on supporting TE-like localized modes in the optical cavity, which can strongly couple to the material gain of a quantum well.

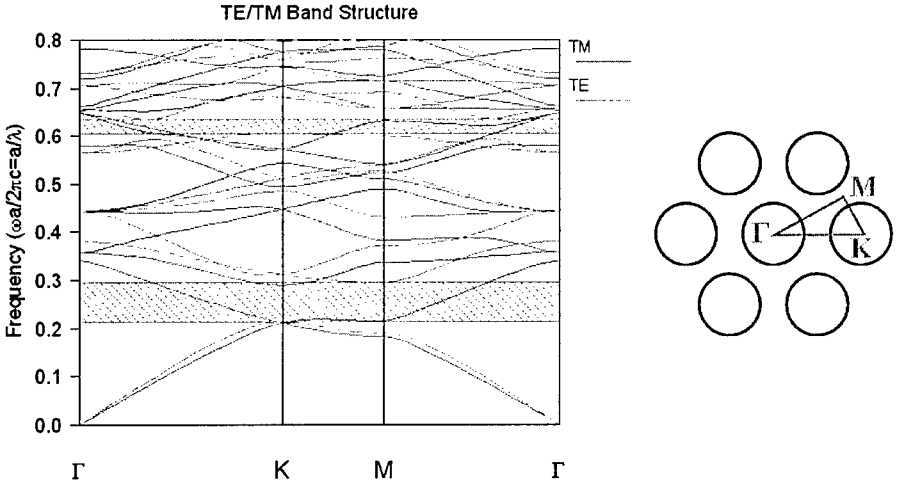

Fig. 3 Photonic band structure of hexagonal lattice. (Red: TE mode; Blue: TM mode). Cross hatched region corresponds to band gaps.

There are two typical photonic crystal patterns: the square lattice and the hexagonal lattice. The square lattice photonic crystal has approximately four times smaller TE-like (even mode) photonic band gap than the hexagonal lattice, but it can produce a high quality whispering-gallery-like mode [5]. Because of the larger band gap and flexibility of the photonic crystal structure, many photonic crystal defect lasers reported to date are based on a hexagonal lattice. The simulation of the photonic band structure with a hexagonal lattice using a commercial software package, BandSOLVE [6], is shown in Figure 3. In the photonic band diagram, the vertical axis represents a normalized frequency a/λ to describe the photon frequencies, where λ is the wavelength in air. The horizontal axis corresponds to an in-plane wave vector (k) in the irreducible Brillouin zone of reciprocal lattice [3]. The red hatched regions in Figure 1 represent the photonic band gap for TE mode. The photonic band gap for TM mode does not exist in this photonic crystal structure.

Unlike the infinite thickness structure shown in Figure 3, there is a light line (green line) in the photonic band structure for the photonic crystal slab with a finite thickness as shown in Figure 2. The light line divides guided modes and leaky modes generated from the slab. The region above the light line corresponds to modes which leak energy out of the slab into the surrounding material. The modes in the bands below the light line can propagate in the slab without energy loss. Since the light line can be simply interpreted as the linear dispersion curve of a photon in the surrounding material, the slope of the light line represents the refractive index ratio between the slab and surrounding material. As the index difference is larger, the slope increases. In Figure 2, the red hatched region represents the photonic band gap of TE-like mode. The photonic band gap for TM-like mode does not exist in this structure. In the air-suspended photonic crystal with a 210 nm thick slab, the photonic band gap for the TE-like mode exists from 0.255 to 0.342 a/λ shown in Figure 4 (a).

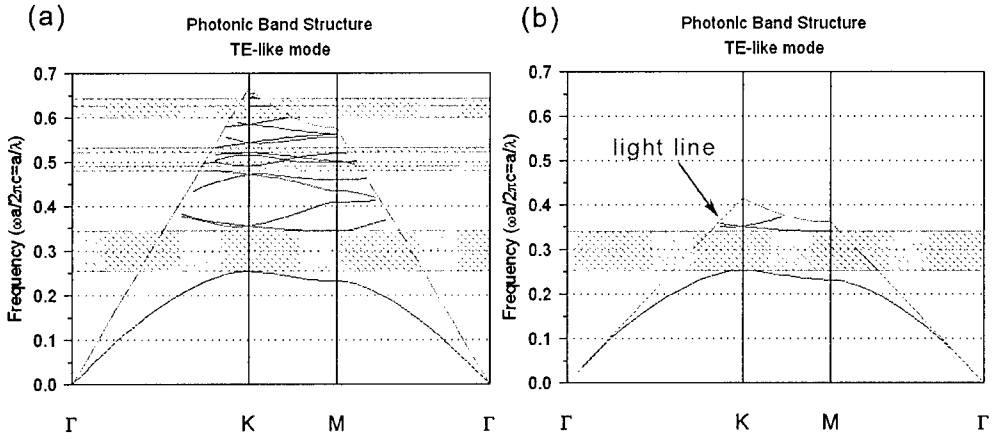

Fig. 4. Photonic band structure of hexagonal lattice with a finite thickness (210 nm). (a) air-semiconductor-air structure and (b) air-semiconductor-oxide cladding structure.

When an oxide cladding layer (n = 1.6) is incorporated below the semiconductor slab for electrical injection, it breaks the air-semiconductor-air symmetry of the structure. The light line shrinks down due to the smaller index difference in the oxide cladding structure as shown in Figure 2 (b). The oxide cladding structure increases the radiation loss into the oxide layer corresponding with the lesser slope of the light line. Unlike the photonic band structure of the air suspended membrane, most optical modes lie above the light line in Figure 2 (b). Since these modes are not completely guided within the slab [7], the optical loss increases in the photonic crystal.

2.2) Defect Cavity Resonant Mode Calculation

Once the photonic band structure is obtained, the next step is finding the resonant frequencies of the cavity. A commercial 3-D FDTD simulation package, FullWAVE [6] is used to calculate resonant frequencies from our cavity design. Figure 3 (a) shows the relative intensity profile as a function of frequency for the H2 defect cavity structure with 320 nm lattice spacing and r/a = 0.35. In this dissertation, the number following H, which means "Hexagonal", represents the number of missing holes in a single side of the hexagon defect. Electric field intensity profiles of in-plane propagation of the resonant mode are obtained as a function of time as shown in Figure 3 (b). The in plane electric field profile indicates the symmetry of a specific resonant mode. Many of simple defect structures like H1, and H2 produce multiple resonant modes, but the cavity modes matching the gain spectrum are typically dipole modes. Moreover, modification of the nearest holes around the defect has been developed to create new resonant modes like monopole and hexapole [8], or to suppress unwanted resonant modes [9, 10].

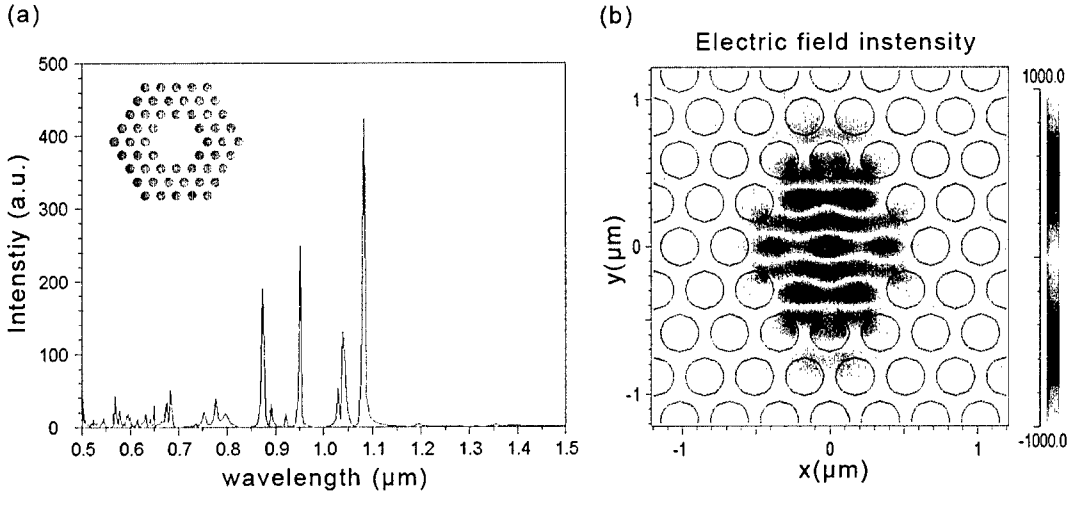

Fig. 5 (a) Resonant frequencies of the H2 cavity. (b) Electric field intensity profile.

The strongly confined electric field profile of the resonant mode in Figure 3 (b) indicates that spatial gain localization within the defect region of the photonic crystal allows for efficient coupling of the optical mode to the gain medium. We would like to apply novel semiconductor growth techniques in order to localize the gain media such as quantum dots and quantum wells. Furthermore, we can engineer the position of the gain medium within the defect region to optimally overlap the electric field profile. Thus, the optical emission from the gain media in the nanocavity can be efficiently coupled to the cavity modes, which can be lithographically engineered.

Design Parameters

Since the peak emission wavelength of the InGaAs/GaAs quantum well used in this thesis is 1025 nm, the lattice spacing (a) can be determined from the normalized frequency (a/_) in the photonic band structure. We need to decide the thickness of the slab to maximize the photonic band gap because both lattice spacing and radius can be lithographically modified, but the thickness of the slab is fixed after it is epitaxially grown. For a given r/a ratio and known emission wavelength from the material gain spectrum, the photonic band gap will be maximized when the thickness of the slab is 0.5-0.6 a [11]. For a given thickness of the slab, as the r/a ratio increases, the size of the photonic band gap is larger, and the center frequency of the photonic crystal band gap tends to increase because the average refractive index is lower due to the larger air fraction [3,4]. However, the realizable maximum value of the r/a ratio is less than 0.35 because of the mechanical stability of the membrane structure and fabrication limitations. Thus, the r/a ratio of the photonic crystal and the thickness of the membrane in our cavity design are fixed to 0.32 and 210 nm, respectively.

Photonic crystal fabrication

Device Fabrication Overview

Fabrication processes of photonic crystal defect cavities have been developed using air-suspended slab structures because of the process complexity of the regrown structure which includes two electron beam lithography steps and a regrowth process. We first implemented the photo-pumping cavity structures as a preliminary step toward an electrical current injection structure. The electron beam lithography, sequential dry etches, and undercut wet etch of the photonic crystal cavities will be discussed in the following sections.

Optical Pumping Structure

The epitaxial structure for optically pumped photonic crystal cavities consists of an 220 nm thick GaAs membrane containing multiple stacks of self-assembled quantum dots and a 1 μm thick Al0.96Ga0.04As sacrificial layer on a semi-insulating GaAs substrate. Unlike the electrical injection structure, this optical pumping structure is undoped. The quantum dots are designed to have a photoluminescence peak near _ 1300 nm. Figure 4 shows the schematic process flow of optically pumped photonic crystal structures. It begins with the completed epitaxially grown material. A dielectric layer is deposited to serve as an etch mask. Electron beam lithography defines photonic crystals with opening structures for the undercut wet etch. Using the dielectric mask, a dry etch perforates the photonic crystal air holes through the membrane and penetrates partially into the sacrificial layer. Finally, an undercut wet etch with a diluted hydrofluoric acid solution removes the sacrificial layer under the photonic crystal and the remaining dielectric mask layer.

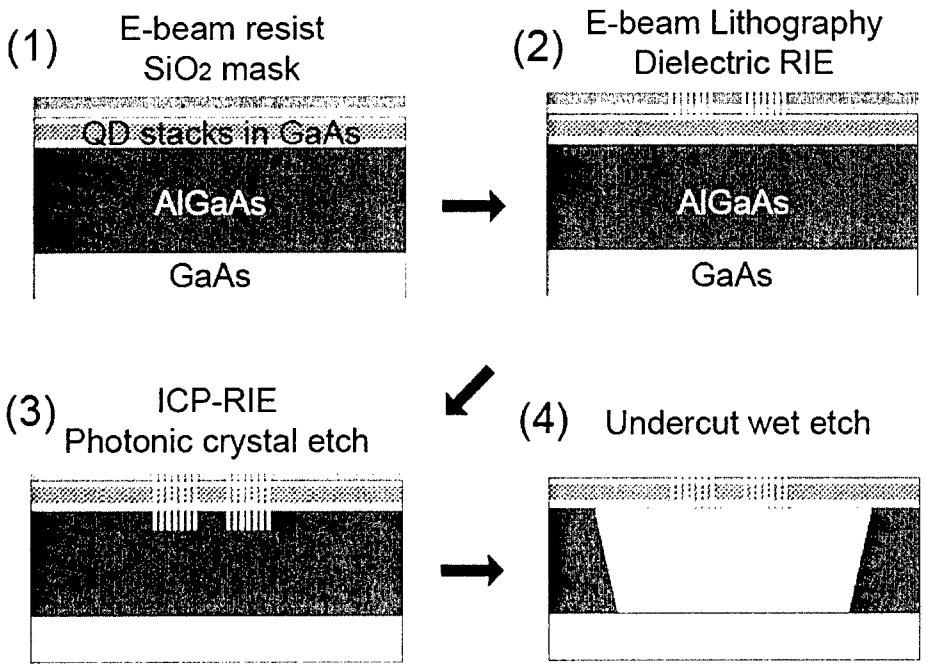

Fig. 6. Fabrication flow of the optically pumped photonic crystal.

Photonic Crystal Definition

Two nano-lithographic approaches to define photonic crystal cavities have been developed. First, a focused ion beam (FIB) system is used to directly mill the photonic crystal patterns on a dielectric layer, which is deposited for the etch mask [1]. The photonic crystal cavities are transferred to the GaAs membrane by a dry etch with an inductively coupled plasma reactive ion etch (ICP-RIE) system. The primary advantage of FIB nano-patterning is that FIB can directly create patterns into a dielectric layer or a semiconductor without a resist. FIB can also define patterns on the sample with height variations such as a mesa and a ridge because it does not require a spin-coated resist. Thus, the FIB patterning process is easy to develop prototype devices. In addition, FIB can achieve gray scale patterns by controlling the beam current and milling time, whereas EB lithography is a binary process. FIB can even allow patterns to perforate a metal layer. This is a unique capability of FIB patterning. This technique can also be applied to create a periodic pattern or a single hole in the metal layer for studying surface plasmonic devices. However, there are several disadvantages of FIB nano-patterning for photonic crystal fabrication. The r/a ratio of the actual pattern in the semiconductor is smaller than that desired because the sidewall of the FIB milled pattern in the dielectric mask layer is not cylindrical but more conical. The FIB lithographic pattern relies sensitively on the conditions of electron and ion beam, so reproducibility and uniformity are not as good as electron beam lithography of described below. Furthermore, the field of view in the scanning electron microscope (SEM) of the FIB system limits the pattern area. It also takes an enormous time to create multiple patterns due to the serial patterning process.

Electron beam lithography has also been used for the photonic crystal pattern definition. The electron beam lithography requires an electron beam resist. The electron beam pattern written on the resist is transferred into a dielectric layer by a Freon reactive ion etch. An ICP-RIE is then performed to create the photonic crystal pattern in the semiconductor as previously described. A comparison of holes generated by FIB and electron beam lithography shows that the photonic crystal patterns defined by the electron beam lithography have better uniformity and less roughness. However, electron beam lithography requires stringent process control, dose test, and proximity correction.

Focused Ion Beam Nano-patterning

FIB patterning has been widely used as a versatile maskless lithography technique in numerous fields [1]. FIB systems generally use an ion beam of Ga, focused to a spot size as small as 7 nm in diameter, and accelerated up to 50 keV energies. Since FIB patterning saves process steps and time, it can be exploited to develop prototypes of

both electrical and optical devices [1–6]. However, FIB nanolithography is generally a destructive method to generate patterns directly on the surface with small lateral dimensions. Therefore, it requires a milling strategy dependent on the geometry of the pattern and inclusion of material related issues such as redeposition and material swelling [7, 8]. The major problems occurring during FIB patterning are sputtered material redeposition and incident ion beam contamination [9], that may alter the material properties. The sputtered material redeposition can be eliminated by using dielectric layers, and the effect of incident Ga ions is not critical in GaAs based materials. The resolution of the defined features is fundamentally limited by the spot size of incident ion beam, which is typically 10 nm in diameter. Recently, many optoelectronic devices employ subwavelength-scale structures, such as diffraction gratings, distributed Bragg reflectors (DBRs), 1- or 2-dimensional photonic crystals, and surface plasmon devices. It can be difficult to create these nano-structures using conventional optical photolithography. Thus, nano-scale lithography techniques such as electron beam lithography and FIB patterning are necessary for their fabrication.

FIB experiments are performed with an FEI Strata DB-235 Dual-beam FIB system at the Materials Research Laboratory, which is comprised of a high-resolution field emission scanning electron microscope and a scanning Ga metal ion beam column. The 30 keV ion column with a Ga metal ion source provides ion beam current ranging from 1 pA to 40 nA. The Ga ion beam resolution is 7 nm at 1 pA beam current with a fixed 30 keV accelerating voltage. The beam spot size and resolution will vary with the ion beam current.

In order to develop the FIB lithography technique of photonic crystal nano-cavities, we first create simple patterns with similar scale as the photonic crystal air holes using a simple structure with an epitaxially grown 100 nm thick GaAs layer on a GaAs substrate. Approximately 50 °A thick film of titanium (Ti) is deposited in order to avoid surface charging while the samples are exposed to electron or ion beams, which could deform the ion beam shape. Similarly, a gold palladium alloy is typically used for silicon based materials. This Ti layer can be easily removed in a buffered oxide etch solution without damaging the GaAs materials. Figure 5 shows a 10 x 10 array of holes that are patterned using FIB with ion beam current of 50 pA. The measured period and diameter of holes are 150 nm and 80 nm, respectively. The designed ratio of the hole diameter to the hole period is 0.35, and thus the patterned holes in Figure 5 are broadened by about 50 %. The depth of the holes is measured to be 125 nm using a FIB milled cross section image, as shown in the inset of Figure 5. The shape of the holes is affected by the aperture of the ion beam column. The diameter and depth of the hole can be controlled by changing the dwell time and beam current. For a fixed total milling time, when reducing the dwell time, the number of ion beam scans for each hole increases. Repeated scans of the ion beam into a hole results in broadening the hole. As the beam current increases, the aperture and the spot size of the ion beam increases. Thus, the size of the holes becomes larger. Therefore, a long dwell time with the smallest beam current is the best condition for patterning the smallest nanostructures using FIB. However, this also requires long milling times and thereby we do not consider such cases in this study.

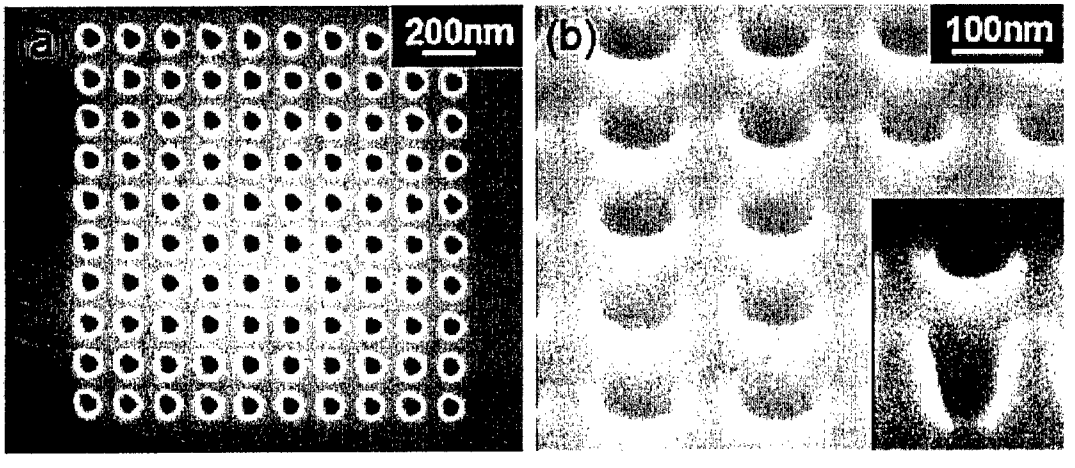

Fig. 7 (a) SEM of 10x10 array of FIB holes. (b) Close up of hole profile.

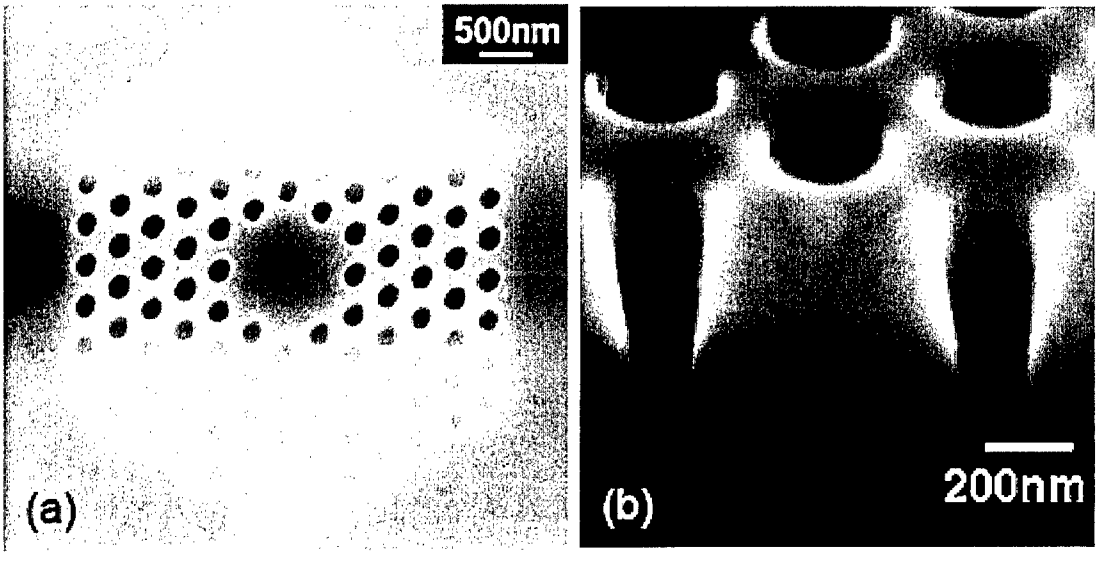

Fig.8. (a) SEM image of photonic crystal cavity defined by FIB; (b) close up image of holes.

In addition to the sputtered material redeposition, another drawback using FIB is the typical conical profile of the feature due to the ion beam shape and the sputtering process. As the size of the pattern is smaller, this effect is more serious as shown in Figure 6. Vertical and smooth sidewalls of the hole etch profiles are desirable in many optical or electrical devices. To achieve an anisotropic hole shape, we have developed a process using FIB patterning of a thin dielectric mask layer followed by a dry etch process [1]. This approach yields vertical sidewalls and also solves the redeposition problem. A SiO2 or Si3N4 layer protects the sample surface from the redeposition, and serves as the etch mask for the dry etch process. A thin Ti layer can be deposited on the dielectric layer to avoid surface charging during FIB patterning. After the FIB patterning is performed, this patterned dielectric mask is used for a dry etch. The ICP-RIE process is controlled to give proper hole depth and profile, and also removes the remaining Ti layer and redeposited materials on the dielectric layer. The dielectric mask layer can then be selectively removed. We observe that etched holes retain their cylindrical shape in deeper etches as compared to direct FIB etching cases, where the holes take on a more conical appearance.

The sample shown in Figure 6 consists of 400 nm GaAs and 600 nm AlAs layers epitaxially grown on the GaAs substrate. A 100 nm thick SiO2 is deposited by plasma enhanced chemical vapor deposition for the etch mask with 50 °A thick Ti layer on top. FIB milling is performed at 100 and 300 pA ion beam current with 30 keV Ga ion beam. A simple photonic crystal pattern can be directly transferred to Ti/SiO2 mask under the precise control of FIB. ICP-RIE with SiCl4/Ar plasma then propagates the air holes into the semiconductor slab using the FIB patterned dielectric mask. During the ICP-RIE process, most of the Ti layer is also etched away. The remaining Ti/SiO2 layer can be easily removed by a diluted hydrofluoric acid etch which also removes the 600 nm AlAs sacrificial layer under the GaAs membrane. Figure 6 shows an undercut etched photonic crystal structure. The lattice spacing and diameter of holes are 350 nm and 200 nm, respectively. Since the sidewall of the FIB milled pattern in the Ti/SiO2 layer is not very cylindrical, the measured r/a ratio of the actual pattern in the slab is smaller than that desired (_ 250 nm).

The FIB lithographic pattern relies sensitively on the conditions of the ion beam column, so reproducibility and uniformity are not as good as those of electron beam lithography. Furthermore, the field of view in scanning electron microscope of the FIB limits the pattern area. It is difficult to create more than about 10 photonic crystal periods in a single pattern. The primary advantage of FIB nano-patterning is that FIB can directly generate mask patterns into a dielectric layer or a semiconductor without a resist.

Electron Beam Lithography

Electron beam (EB) lithography has been commonly used to define nano-scale patterns. Both EB lithography and FIB patterning can create nano-scale patterns, but each method has performance advantages and inherent limitations.

The EB lithography process is done using an EB resist such as polymethylmethacrylate (PMMA), which transfers a pattern to another mask material. The EB lithography can align the multiple levels with alignment marks and can write a larger area in a relatively shorter time than FIB. The photonic crystal patterns defined by the EB lithography show better uniformity and less feature roughness than FIB patterns. Therefore, we primarily use the EB lithography for our fabrication of electrically injected photonic crystals.

After the regrowth process discussed in the Chapter 3.2, the sample is rinsed in a concentrated hydrofluoric acid solution for 15 sec to remove amorphous GaAs grown on the SiO2 mask layer and the remaining SiO2 layer at the alignment marks for the second electron beam lithography. A 100 nm thick layer of SiO2 is deposited by plasma-enhanced chemical vapor deposition to serve as an etch mask. A 100 nm thick 3% 950-K PMMA is spun onto the sample, and baked at 200 _C for 2 min. Electron beam lithography is performed at 100 pA beam current by a JEOL JBX-6000FS electron beam lithography system at the Micro and Nanotechnology Laboratory. The photonic crystal cavities and oxidation trenches are simultaneously written for self-alignment. The PMMA is developed in a 1 : 2 = methyl-isobutyl-ketone : isopropanol solution for 90 sec, and rinsed in isopropanol for 30 sec. At this point, the patterned quantum well must be placed within the photonic crystal defect defined by the EB lithography.

Figure 7 shows a H3 photonic crystal cavity defined on the PMMA layer. The lattice spacing of the photonic crystal is 250 nm, which is the smallest one in the layout. The r/a ratio of _ 0.34 is measured. The air holes are uniform from the center to the outer 12th period by using proximity correction, which increases the dose in the outer most four periods of the photonic crystal pattern. The photonic crystal patterns are then transferred to the SiO2 layer using a Freon 23 (CHF3) reactive ion etch (RIE) system. The etch selectivity of 1:1.5 for PMMA is achieved when etching a photonic crystal pattern into the 100 nm thick SiO2 layer. The relatively poor selectivity of the PMMA limits the SiO2 thickness to _ 120 nm. The PMMA is stripped in a 1 : 1 = methylene-chloride : methanol solution, and the residual PMMA is removed by O2 descum for 3 min.

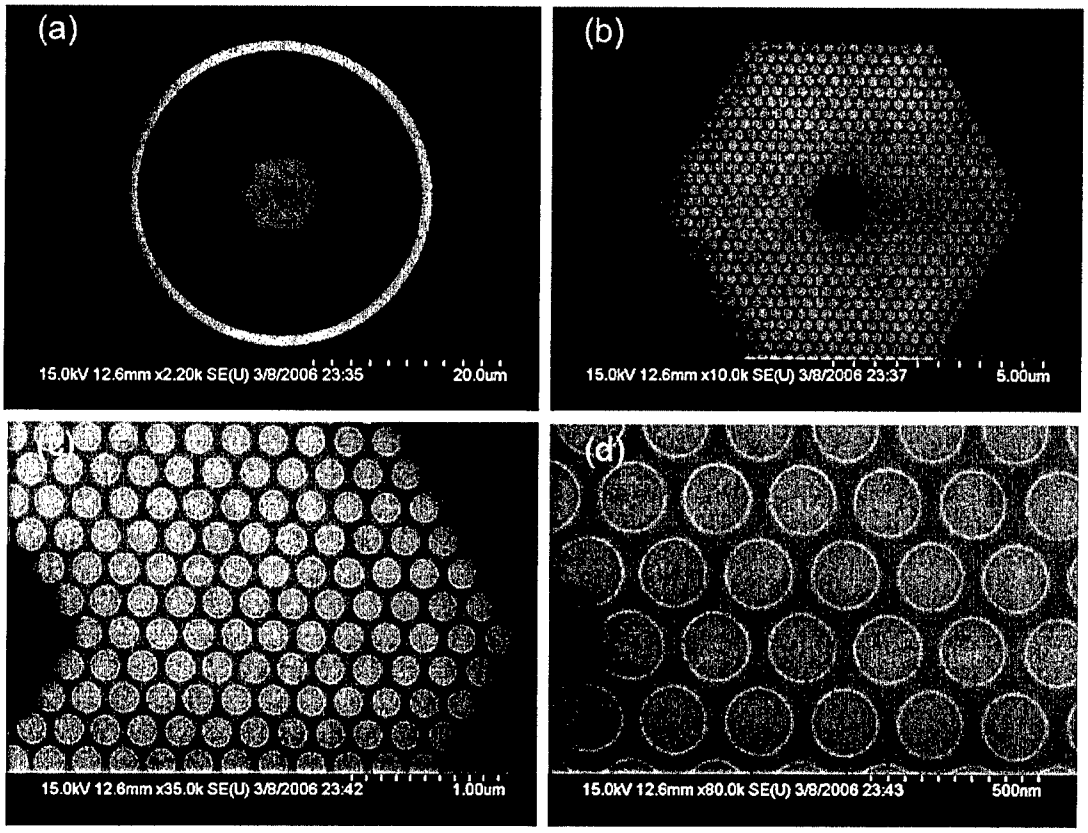

Fig. 9. SEM images of H3 photonic crystal pattern on the PMMA layers.

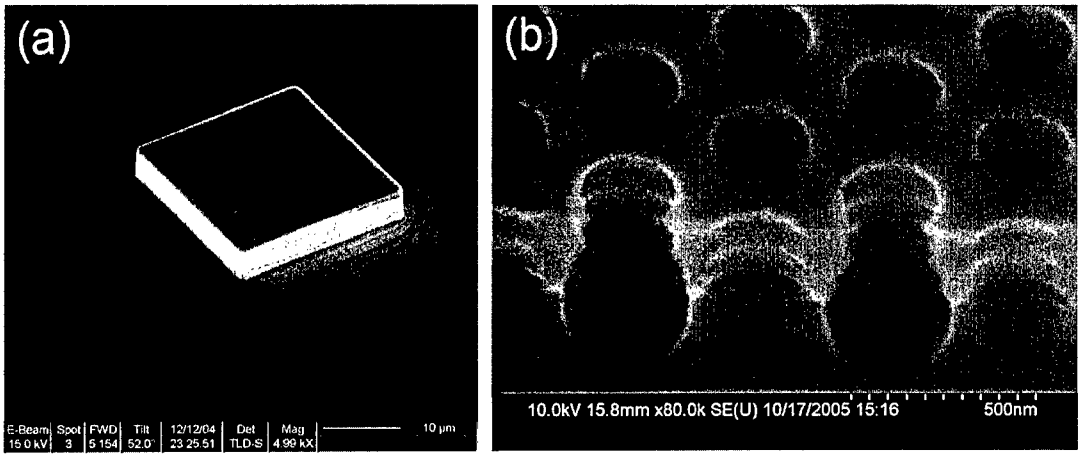

Fig. 10. SEM image of a (a) mesa and (b) Photonic crystal hole.

Inductively Coupled Plasma Reactive Ion Etch

The photonic crystal nanocavities require an anisotropic dry etch process with a SiO2 mask to GaAs. A Plasma Therm SLR-770 ICP-RIE system in Micro and Nanotechnology Laboratory is used for all etches described in the following. Since an etch depth of more than _ 500 nm is sufficient for both air-suspended and oxide cladding structures, an approximately 100 nm thick SiO2 layer is needed for the greater than 1 : 10 dry etch selectivity of the SiO2 mask to GaAs. The etched air holes with vertical and smooth sidewalls will influence the cavity quality and the optical performance of the devices. Rough sidewalls would increase scattering loss and angled sidewalls would cause radiative loss of the unconfined modes because of the broken vertical symmetry. From the aspect of device fabrication, the dry etch profile also influences the mechanical stability of the air-suspended membrane structure during the sequential undercut wet etch process.

Figure 8 shows that the etch profile of the photonic crystals in the GaAs/AlGaAs material system is quite different from that of mesa structures etched by ICP-RIE with the same process condition. We typically etch the mesa structures for VCSELs with a SiCl4 : Ar gas ratio of 2 : 2.5 sccm at a chamber pressure of 1.5-2 mT. The ICP and RF powers are 110 W and 35 W, respectively. The etch rate is 400 nm/min, and the etch selectivity is generally greater than 1 : 20 for a SiO2 mask. In Figure 8 (a), the mesa structure is etched to greater than 4 μm depth with smooth and vertical sidewalls. On the other hand, the photonic crystal air holes in Figure 8 (b) are severely undercut using the same process condition. We also observe that the etch rate is over 50% slower when the feature size is smaller than 200 nm, and the etch profile is no longer vertical and smooth. Thus, we have developed an optimized ICP-RIE process for the photonic crystal structure with the optical pumping material as described in Section 4.2.1.

Optimization etched are done with a fixed chamber pressure of 2 mT. All the etches in this thesis are performed at room temperature. The SiCl4 : Ar gas ratio, ICP power, and RF power are varied. After 3 min etch, the samples are cleaved, and then observed in a Hitachi S4800 SEM. An initial etch profile is shown in Figure 8 (b). To improve the anisotropy of the etched air holes, ICP and RF powers are increased while keeping the DC bias at 120 V. Figure 10 are taken from three different samples etched using the same conditions. They all show smooth and vertical etch profile without deterioration of the SiO2 mask. We primarily use this etch condition for both air-suspended photonic crystal structures.

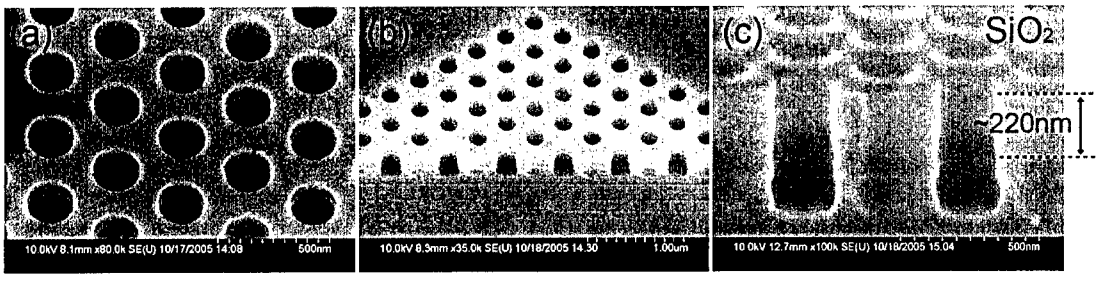

Fig. 11. Top view (a), side view (b) and cross section view (c) of optimized ICP-RIE photonic crystal etch.

Membrane Formation

The EB lithography and sequential dry etch processes can reproducibly define the photonic crystal structure into the semiconductor membrane. Simultaneously, a large refractive index difference in the vertical dimension is required for guiding the optical mode. There are several ways to achieve this, such as an undercut wet etch to build a air-suspended structure [10], incorporating an oxide cladding layer underneath the slab [11], and wafer bonding to lower refractive index materials [12,13]. The air-suspended structures can create a larger TE-like photonic band gap than the oxide or low index material under the membrane, so most of optically-pumped photonic crystal lasers are air-suspended structures.

In order to fabricate the free standing slab, a 220 nm thick GaAs membrane including a InGaAs QW layer is epitaxially grown on 3 μm thick Al0.60Ga0.40As sacrificial layer, which can be selectively etched by a concentrated HF solution [15]. The AlGaAs layer with over 90% Al-content can also be selectively wet etched by a diluted phosphoric acid [16] or a diluted HF solution [17]. The undercut etch is performed through the ICP-RIE etched photonic crystal air holes and U-shape opening around the photonic crystal as shown in Figure 11 (c) to prevent the membrane from bending during the wet etching and drying [16]. The 220 nm thick GaAs membranes are very fragile, so they are easy to break or collapse down to the substrate due to the surface tension during the wet etching. To avoid either membrane collapse or bowing, the samples etched by a diluted HF solution are first rinsed in deionized (DI) water, and transferred into methanol and isopropylalcohol (IPA) mixture. The samples are then soaked in a hot methanol for a while. Finally, the solvent is allowed to evaporate without any treatment. Figure 11 shows L3 photonic crystal cavity, formed by three missing air holes in a line within a hexagonal photonic crystal lattice, as previously mentioned in Chapter 1.3. The air holes at both edges are displaced by 0.15 a to increase the quality factor [18]. An array of L3 cavities are designed to have 32 patterns from a = 310 nm to a = 403 nm with a 3 nm increment. The r/a ratio of 0.31 are measured from the SEM image. The FIB milled image in Figure 11 (d) shows a clean undercut with vertical and smooth sidewalls. A slight bowing of the membrane in this image has been created during the FIB milling.

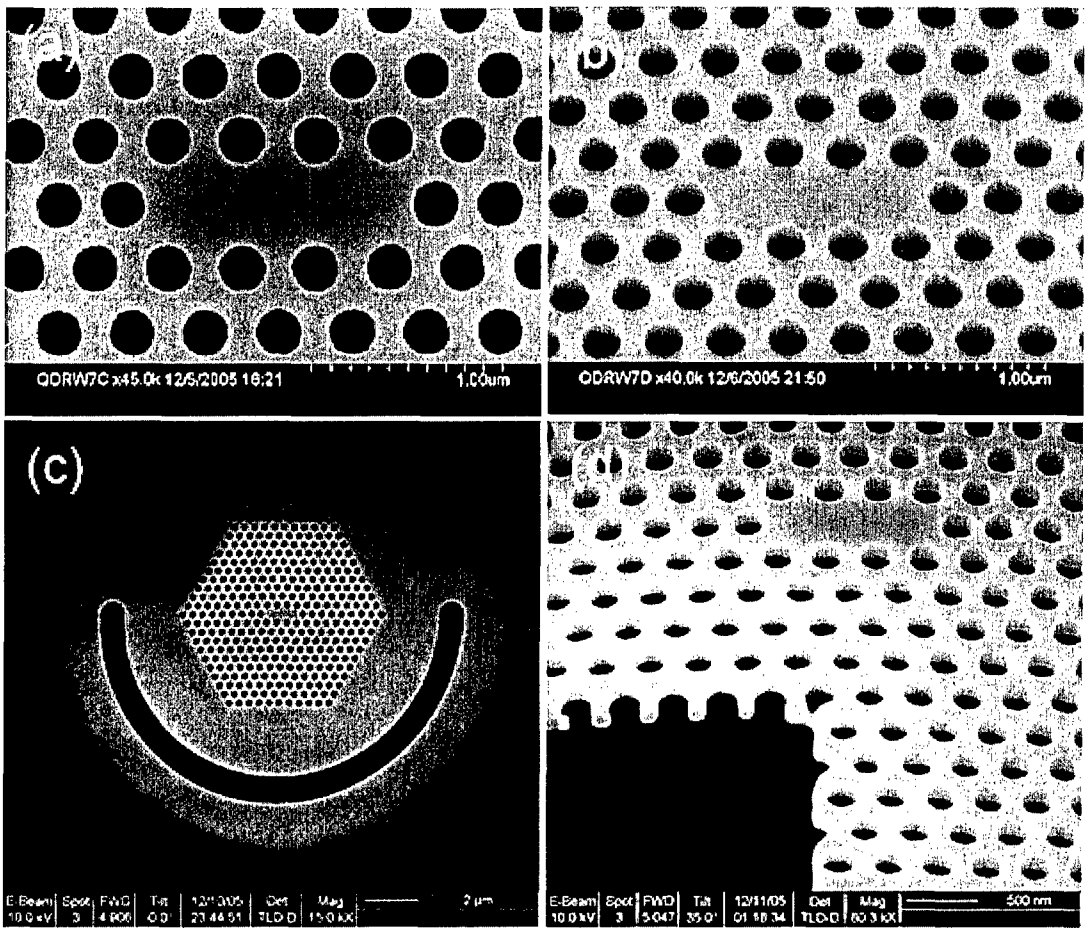

Fig. 12. SEM images of L3 photonic crystal.

References

1] M. Plihal and A. A. Maradudin, "Photonic band structure of two-dimensional systems: the triangular lattice," Phys. Rev. B, vol. 44, pp. 8565-8571, 1991.

[2] G. Mur, "Total-field absorbing boundary conditions for the time-domain electromagnetic field equations," IEEE Transactions on Electromagnetic Compatibility, vol. 40, pp. 100-102, 1998.

[3] J. D. Joannopoulos, R. D. Meade, and J. Winn, Photonic Crystals: Modeling theFlow of Light, Princeton Univ. Press, Princeton, NJ, 1995.

[4] O. Painter, J. Vuckovic, and A. Scherer, "Defect modes of a two-dimensional photonic crystal in an optically thin dielectric slab," J. Opt. Soc. Am. B, vol. 16, pp. 275-285, 1999.

[5] H.Y. Ryu, J.K. Hwang, and Y.H. Lee, "The smallest possible whispering-gallerylike mode in the square lattice photonic-crystal slab single-defect cavity," IEEE J. Quantum Electron., vol. 39, pp. 314-322, 2003.

[6] RSoft Design Group, Inc. (2002), http://www.rsoftdesign.com

[7] C. Kim, W. J. Kim, A. Stapleton, J. R. Cao, J. D. O'Brien, and P. D. Dapkus," Qualitiy factors in single-defect photonic crystal lasers with asymmetric cladding layers," J. Opt. Soc. Am. B, vol. 19, pp. 1777-1781, 2002.

[8] H.G. Park, J.K. Hwang, J. Huh, H.Y. Ryu, S.H. Kim, J.S. Kim, and Y. H. Lee, "Characteristics of modified single-defect two-dimensional photonic crystal lasers," IEEE J. Quantum Electron., vol. 38, pp. 1353-1365, 2002.

[9] O. Painter, R. K. Lee, A. Scherer, A. Yariv, J. D. O'Brien, P. D. Dapkus, and I. Kim, "Two-dimensional photonic band-gap defect mode laser," Science, vol. 284, pp. 1819-1821, 1999.

[10] J. Vuckovic, M. Loncar, H. Mabuchi, and A. Scherer, "Optimization of the Q factor in photonic crystal microcavities," IEEE J. Quantum Electron., vol. 38, pp. 850-856, 2002.

[11] S. G. Johnson, S. Fan, P. R. Villeneuve, J. D. Joannopoulos, and L. A. Kolodziejski, "Guided modes in photonic crystal slabs," Phys. Rev. B, vol. 60, pp. 5751-5758, 1999.
[12] Y. K. Kim, A. J. Danner, J. J. Raftery, Jr., and K. D. Choquette,"Focused ion beam nano-patterning for optoelectronic device fabrication," IEEE Journal of Selected Topics in Quantum Electronics, vol. 11, no. 6, pp. 1292-1298, 2005.
[13] O. Yavas, C. Ochiai, M. Takai, Y. K. Park, C. Lehrer, S. Lipp, L. Frey, H. Ryssel, A. Hosono, and S. Okuda, "Field emitter array fabricated using focused ion and electron beam induced reaction," J. Vac. Sci. Technol. B, vol. 18, pp. 976-979, 2000.
[14] Y. Fu, K. A. B. Ngoi, and N. S. Ong,"Diffractive optical elements with continuous relief fabricated by focused ion beam for monomode fiber coupling," Opt. Express, vol. 7, pp. 141-147, 2000.
[15] C. Ochiai, A. Sawada, H. Noriyasu, M. Takai, A. Hosono, and S. Okuda, "Wedge emitter fabrication using focused ion beam," J. Vac. Sci. Technol. B, vol. 19, pp. 904-906, 2001.
[16] A. J. Danner, N. Yokouchi, J. J. Raftery Jr., K. D. Choquette, "Focused ion beam post-processing for single mode photonic crystal vertical cavity surface-emitting lasers," Device Research Conference, Salt Lake City, UT, 2003.
[17] K. Wang, P. Filloux, N. Paraire, P. Roca I Cabarrocas, and P. Bulkin, "Twodimensional photonic crystals by focused-ion-beam etching of multilayer membranes," J. Vac. Sci. Technol. B, vol. 21, pp. 966-969, 2003.
[18] A. Lugstein, B. Basnar, and E. Bertagnolli, "Study of focused ion beam response of GaAs in the nanoscale regime," J. Vac. Sci. Technol. B, vol. 20, pp. 2238-2242, 2002.
[19] A. Lugstein, B. Basnar, G. Hobler, and E. Bertagnolli, "Current density profile extraction of focused ion beams based on atomic force microscopy contour profiling of nanodots," J. Appl. Phys., vol. 92, pp.4037-4042, 2002.
[20] J. G. Pellerin, G. M. Shedd, D. P. Griffis, and P. E. Russell, "Characterization of focused ion beam micromachined features," J. Vac. Sci. Technol. B, vol. 7, pp. 1810-1812, 1989.
[21] S. Yoshimasa, I. Naoki, C. Niclas, A. Kiyoshi, K. Noriko, and I. Kuon, "Fabrication and characterization of different types of two-dimensional AlGaAs photonic crystal slabs," J. Appl. Phys., vol. 91, pp. 922-929, 2002.
[22] T. Yu, S. Yoshimasa, I. Naoki, Y. Tao, A. Kiyoshi, W. Yoshinori, I. Kuon, M. Taishi, M. Kazuya, and I. Koji, "Fabrication and characterization of AlGaAs-based photonic crystal slab waveguides by precisely controlled self-aligned selective-oxidation process," Jpn. J. Appl. Phys., vol. 42, pp. 7331-7338, 2003.
[23] J. R. Cao, W. Kuang, Z.J. Wei, S. -J. Choi, H. Yu, M. Bagheri, J. D. O'Brien, and P. D. Dapkus, "Sapphire-bonded photonic crystal microcavity lasers and their far-field radiation patterns," Photon. Tech. Lett., vol. 17, pp. 4-6, 2005.
[24] M. H. Shih, W. Kuang, T. Yang, M. Bagheri, Z.J. Wei, S. -J. Choi, L. Lu, J. D. O'Brien, and P. D. Dapkus, "Experimental characterization of the optical loss of sapphire-bonded photonic crystal laser cavities," Photon. Tech. Lett., vol. 18, pp. 535-537. 2006.
[25] K. D. Choquette, K. M. Geib, C. I. H. Ashby, R. D. Twesten, O. Blum, H. Q. Hou, D. M. Follstaedt, B. E. Hammons, D. Mathes, and R. Hull, "Advances in selective wet oxidation of AlGaAs alloys," IEEE J. Select. Topics Quantum Electron., vol. 3, pp. 916-926, 1997.
[26] Y. Sugimoto, N. Ikeda, N. Carlsson, K. Asakawa, N. Kawai, and K. Inoue, "AlGaAsbased two-dimensional photonic crystal slab with defect waveguides for planar lightwave circuit applications," IEEE J. Quantum Electron., vol. 38, pp. 760-769, 2002.
[27] T. Yang, S. Lipson, J. D. O'Brien, D. G. Deppe,"InAs quantum dot photonic crystal lasers and their temperature Dependence," Photon. Tech. Lett., vol. 17, pp. 2244-2246, 2005.
[28] C. Reese, B. Gayral, B. D. Gerardot, A. Imamoglu, P. M. Petroff, and E. Hu, "High-Q photonic crystal microcavities fabricated in a thin GaAs membrane," J. Vac. Sci. Technol. B, vol. 19, pp. 2749-2752, 2001.
[29] Y. Akahane, T. Asano, B. S. Song, and S. Noda, "High-Q photonic nanocavity in a two-dimensional photonic crystal," Nature, vol. 425, pp. 944-947, 2003

c.) Engineered Photonic Crystal Optical Characterization
Optical Pumping Experiment

Undercut etched photonic crystal cavities are optically pumped by either 850 nm or 980 nm diode laser through a single mode fiber with an infrared objective lens (Mitutoyo NIR 50X, NA=0.42) at room temperature. The photoluminescence spectra from the sample are collected into a optical spectrum analyzer (OSA) through the same objective lens. A schematic of the free-space experiment setup used at the University of Southern California (ref) is shown in Figure 12. A typical pulse condition is 16 ns pulse width with a 1-4% duty cycle. The pump beam is focused at normal incident to a 2-3 μm spot size on the sample. The sample is mounted on a xyz-stage, and is observed by an infrared camera.

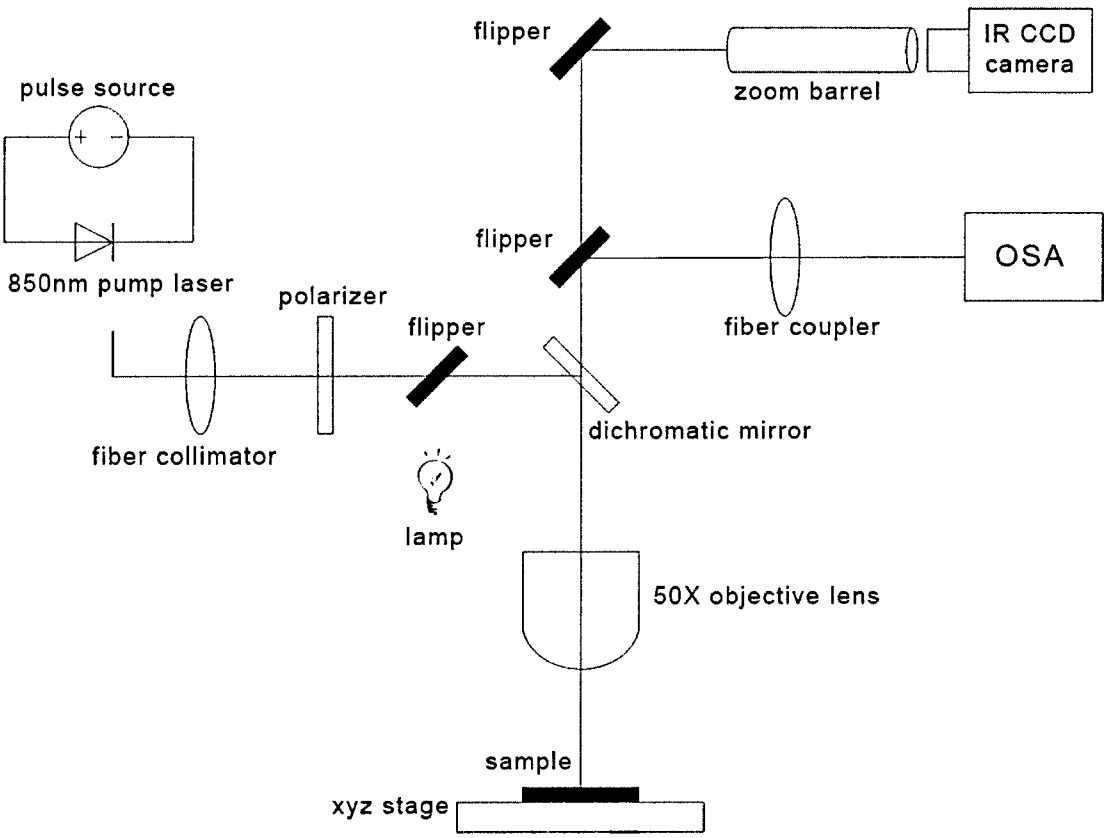

Fig. 12 Schematic of the micro-photoluminescence setup.

Photoluminescence (PL) spectra measured from self-assembled quantum dots and a regrown quantum well are shown in Figure 13. Black curves in both plots represent the PL spectra pumped by a 0.5 mW continuous-wave (CW) beam. Red curves represent the PL spectra pumped by a 12.5 mW pulse laser beam with 16 nm pulse width and 4% duty cycle. The resolution bandwidth of the OSA is set to 5 nm. The quantum dot epitaxial material is grown by Professor Diana Huffaker's group at the University of New Mexico [1]. The material structure consists of a 220 nm GaAs layer containing 3 stacks of self-assembled InGaAs quantum dot layers and a 1 μm Al0.94Ga0.06As undercut layer epitaxially grown on a GaAs wafer. In Figure 13 (a), the ground state, the 1st excited state and the 2nd excited state of the quantum dots are observed from the PL spectra. The emission at the 2nd excited state of the QDs (red curve) is dominant under the pulse pumping due to the saturation of the ground state by a high pump power with a short pulse. The regrown quantum well structure is comprised of the same epitaxial material described in Table 4.1. However, the PL spectra are collected from an unpatterned area. The emission peak of the InGaAs quantum well in Figure 13 (b) is _ 975 nm and does not shift with pulsed excitation. This material is grown for a preliminary experiment to investigate the oxidation rate and the doping concentration in the top contact layer. For the electrical injection photonic crystal structure, the InGaAs quantum well thickness is slightly increased to shift the emission peak toward longer wavelength (_ 1025 nm).

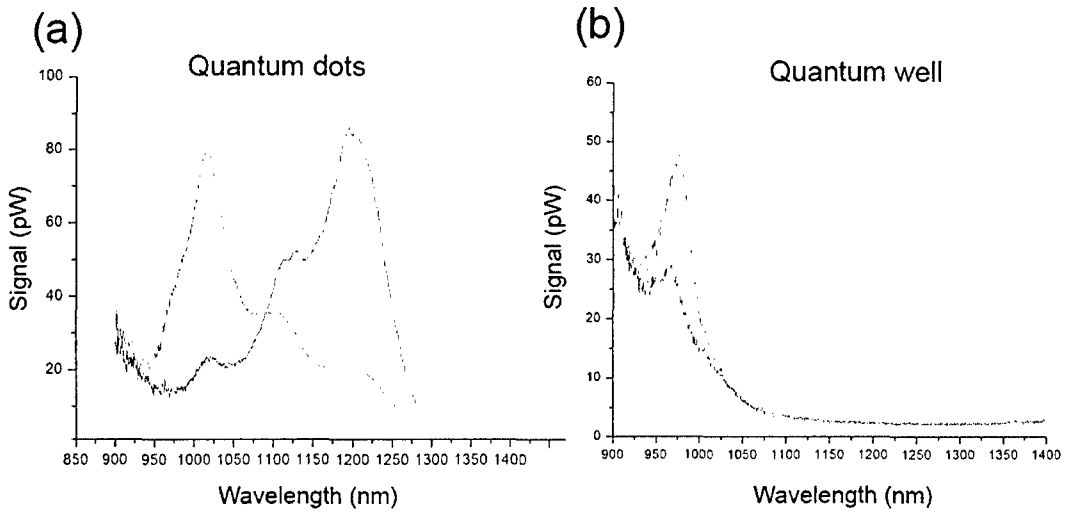

Fig. 13 Photoluminescence spectra pumped by: black 0.5 mW CW; red: 12.5 mW pulsed for (a) quantum dots and (b) quantum wells.

L3 photonic crystal cavity structures are introduced in the 3-stack quantum dot materials to create high Q cavities. The undercut photonic crystal cavity structures are formed through the fabrication procedure described in section 4.2.1. The spectra for 8 devices in Figure 14 (a) are taken under pulsed pumping by 3.75 mW peak power with pulse width 16 ns and 1% duty cycle using the OSA with 5 nm resolution bandwidth. From bottom up in Figure 14 (a), the lattice spacing is 310, 340, 350, 360, 370, 380, 390, and 395 nm respectively. To compare the data in Figure 14 (a), each spectrum is offset by 2 pW. No peaks are observed for devices with a = 320 and 330 nm, which are not plotted.

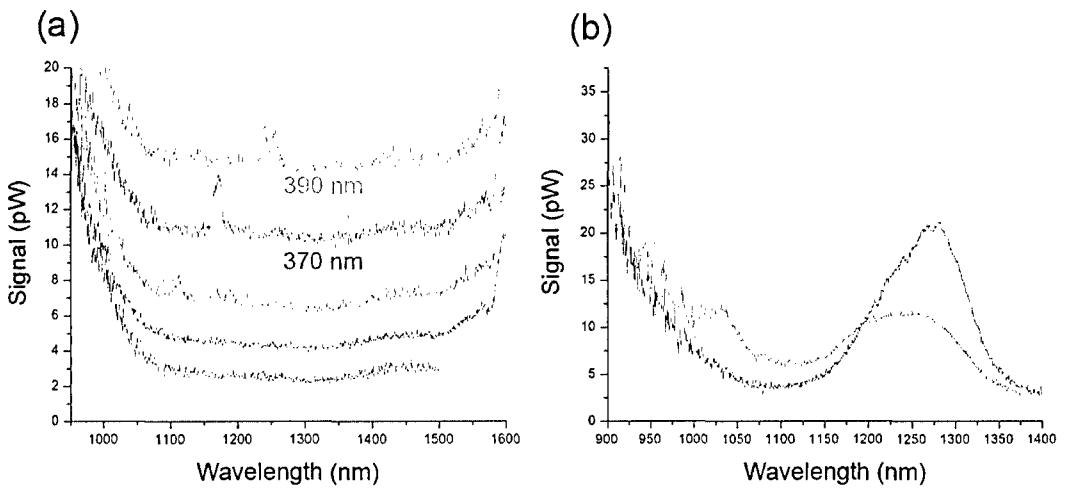

Fig. 14 PL spectra from 3-stack of self-assembled dots (DE2384) (a) L3 photonic crystal cavity (b) unprocessed material.

None of fabricated L3 photonic crystals exhibit lasing because of two probable causes. First, the material gain from the 3-stack QD layers is insufficient to overcome the optical loss induced by the fabrication process such as rough side walls, imperfect undercut wet etch, and membrane bowing. Because of this, we also investigate novel membrane structures containing 6, 8, and 10 layers of strain-compensated self-assembled quantum dots [1, 2] to enhance the material gain, which will be discussed in this Section. The second reason for not achieving stimulated emission is the cavity resonant mode with high quality factor occurs at longer wavelength compared to the PL peak of the gain shown in Figure 14 (b). The spectra show that the doublet peak overlaps the material gain in Figure 14.

However, the high Q cavity mode of the L3 cavity is typically 100 nm longer than the doublet peak [3, 4], which would be thus located at _ 1340 nm. From Figure 14 (b), the emission peak is between 1200 and 1250 nm under CW excitation, which is consistent with the observed cavity emission in Figure 14 (a).

The group at University of New Mexico has recently developed a method to grow greater numbers of quantum dot stacks using a strain compensated growth technique [1, 2]. The L3 photonic crystal cavity structures are introduced in wafers with 6, 8, and 10 stacks of QDs within a 220 nm GaAs membrane. Figure 15 shows a PL spectrum from L3 photonic crystal cavity with the lattice spacing of 382 nm. The device is optically pumped by a 2 mW peak power laser beam with 16 ns pulse and 1% duty cycle at room temperature. The L3 cavity resonant mode is found at the wavelength of 1312 nm, but a lasing does not occur. The bulk PL spectrum in Figure 15 (b) shows a broad emission at the ground state compared to the PL spectrum of the previous 3-stack QD sample as shown in Figure 15 (a) or Figure 14 (b). This may be caused by the nonuniform size distribution of multi-stack quantum dots. In Figure 15 (b), the emissions from the various size of quantum dots are mixed, resulting in an inhomogeneous broadened linewidth (FWHM _ 200 nm). Even if many QD layers are contained in the GaAs membrane, the peak intensity of the PL spectrum does not significantly improve. Therefore, the material gain from multi-stack QDs is insufficient to achieve lasing operation [1].

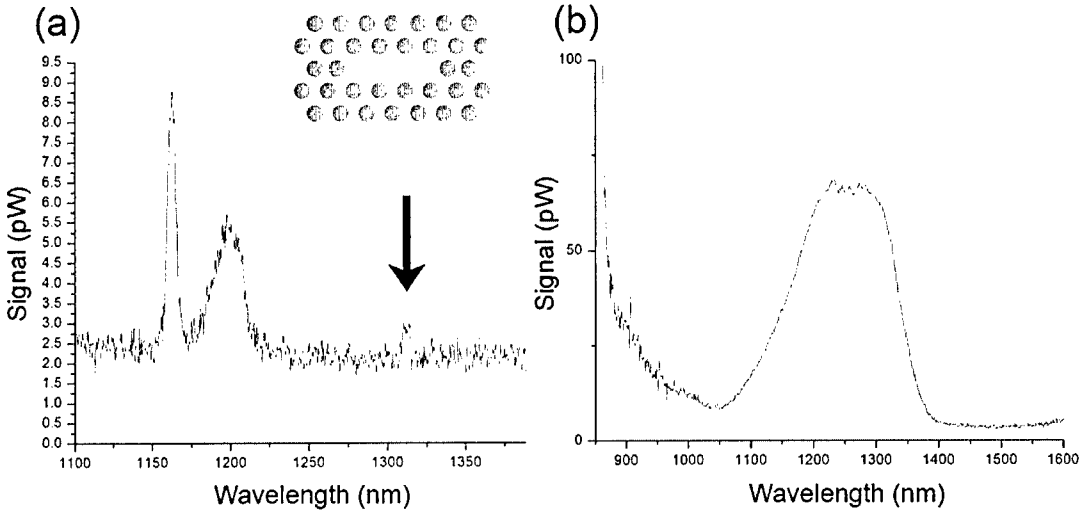

Fig. 15 (a) PL spectra from L3 cavity with lattice spacing of 382 nm. (b) bulk PL spectrum of 8-stack quantum dot wafer (DE2666).

References

[1] N. Nuntawong, Y. C. Xin, S. Birudavolu, P. S. Wong, S. Huang, C. P. Hains, and D. L. Huffaker, "Quantum dot lasers based on a stacked and strain-compensated active region grown by metal-organic chemical vapor deposition," Appl. Phys. Lett., vol. 86, 193115, 2005.

[2] N. Nuntawong, S. Huang, Y. B. Jiang, C. P. Hains, and D. L. Huffaker, "Defect dissolution in strain-compensated stacked InAs/GaAs quantum dots grown by metalorganic chemical vapor deposition," Appl. Phys. Lett., vol. 87, 113105, 2005.

[3] Y. Akahane, T. Asano, B. S. Song, and S. Noda, "High-Q photonic nanocavity in a two-dimensional photonic crystal," Nature, vol. 425, pp. 944-947, 2003

[4] T. Yang, S. Lipson, J. D. O'Brien, D. G. Deppe,"InAs quantum dot photonic crystal lasers and their temperature Dependence," Photon. Tech. Lett., vol. 17, pp. 2244-2246, 2005.

[5] C. Reese, B. Gayral, B. D. Gerardot, A. Imamoglu, P. M. Petroff, and E. Hu, "High-Q photonic crystal microcavities fabricated in a thin GaAs memebrane," J. Vac. Sci. Technol. B, vol. 19, pp. 2749-2752, 2001.

[6] Y. -S. Choi, S. -K. Kim, S. -H. Kim, H. -G. Park, Y. -H. Lee, I. N. Kaiander, F. Hopfer, R. L. Sellin, and D. Bimberg, "Lithographic tuning of photonic-crystal unitcell resonators with InGaAs/GaAs quantum dots emittting at 1.2 μm," J. Vac. Sci. Technol. B, vol. 23, pp. 252-256, 2001.

[7] A. R. Alija, L. J. Martinez, A. Garcia-Martin, M. L. Dotor, D. Golmayo, and P. A. Postigo, "Tuning of spontaneous emission of two-dimensional photonic crystal microcavities by accurate control of slab thickness," Appl. Phys. Lett., vol. 86, 141101, 2005.
[8] M. Plihal and A. A. Maradudin, "Photonic band structure of two-dimensional systems: the triangular lattice," Phys. Rev. B, vol. 44, pp. 8565-8571, 1991.
[9] H. -G. Park, S. -K. Kim, S. -H. Kwon, G. -H. Kim, S. -H. Kim, H. -Y. Ryu, S. -B. Kim, and Y. -H. Lee, "Single-mode operation of two-dimensional photonic crystal laser with central post," Photon. Tech. Lett., vol. 15, pp. 1327-1329, 2003.
[10] H. -G. Park, S. -H. Kim, M. -K. Seo, Y. -G. Ju, S. -B. Kim, and Y. -H. Lee, "Characteristics of electrically driven two-dimensional photonic crystal lasers," IEEE J. Quantum Electron., vol. 41, pp. 1131-1141, 2005.
[11] S. Adachi, GaAs and Related Materials: Bulk Semiconductoring and Super-lattice Properties, World Scientific, Singapore, 1994.

III. List of all publications, conference presentations and inventions.

a.) Huffaker

Publications:

1. *N. Nuntawong, S. Birudavolu,* C.P. Hains, *S. Huang*, H. Xu and **D.L. Huffaker**, "Effect of strain-compensation in stacked 1.3 μm InAs/GaAs quantum dot active regions grown by MOCVD" Appl. Phys. Lett. 85, 3050-3053 (October 11, 2004). ISI times cited: 8
2. *S.Birudavolu, N.Nuntawong, G.Balakrishnan, Y.C.Xin, S.Huang,* S.C. Lee, S.R.J. Brueck, C.P. Hains and **D.L. Huffaker**, "Selective Area Growth of InAs Quantum Dots Formed on a Patterned GaAs Substrate" Appl. Phys. Lett., 85, 2337-2340 (Sept 20, 2004). ISI times cited: 4
3. *S. Birudavolu*, S.Q. Luong, *N. Nuntawong ,Y.C. Xin* ,C.P. Hains and **D.L. Huffaker**, "In-situ Mask Removal in Selective Area Epitaxy using Metal Organic Chemical Vapor Deposition" Journ. Crystal Growth, 277, 1-4, 97 (April 19, 2005). ISI times cited: 0
4. *N. Nuntawong, S. Birudavolu,* C.P. Hains, *S. Huang*, H. Xu and **D.L. Huffaker**, "Quantum Dot Lasers Based on a Stacked and Strain-compensated Active Region Grown by Metalorganic Chemical Vapor Deposition" Appl. Phys. Lett. 86, 193115 (May 16, 2005). ISI times cited:
5. **D. L. Huffaker**, C.P. Hains, *N. Nuntawong Y. C. Xin, P. S. Wong*, L. Yan, S. R. J. Brueck and L. Lester "Temperature-dependent photoluminescence from patterned InAs quantum dots formed using metalorganic chemical vapor epitaxy," Journ. Appl. Phys., 99, 033503 (2005). ISI times cited:
6. *N. Nuntawong, S. Huang*, Y.-B. Jiang, C.P. Hains and **D.L. Huffaker**, "Defect dissolution in strain-compensated, stacked InAs/GaAs quantum dots grown by metalorganic chemical vapor deposition," Appl. Phys. Lett. (Sept 5, 2005). ISI times cited: 1
7. *J. Tatebayashi, N. Nuntawong, Y. C. Xin, P. S. Wong, S. Huang*, L. F. Lester and **D. L. Huffaker** "Ground-state Lasing of Stacked InAs/GaAs Quantum Dots With GaP Strain-compensation Layers Grown by Metalorganic Chemical Vapor Deposition", Appl. Phys. Lett., 88, 221107, May (2006). ISI times cited:
8. *N. Nuntawong, J. Tatebaya*shi, *P.S. Wong* and **D. L. Huffaker**, "Evaluation of Inhomogeneous Strain Reduction in Strain-compensated InAs/GaAs Stacked Quantum Dot Structures Grown by Metalorganic Chemical Vapor Deposition" Submitted to Appl. Phys. Lett.
9. *P.S. Wong, G. Balakrishnan, N. Nuntawong,* L. Xue, J. Tatebayashi, A. Albrecht, P. Rotella, S.R.J. Brueck, and **D. L.** Huffaker, "Controlled Crystal Faceting for Selective InAs Quantum Dot Nucleation", submitted to Nature Materials, 11/20/06. (Invited) *N. Nuntawong, S. Birudavolu,* C.P. Hains, *S. Huang*, H. Xu and D.L. Huffaker, "Effect of strain-compensation in stacked 1.3 μm InAs/GaAs quantum dot active regions grown by MOCVD" Virtual Journal of Nanoscale Science & Technology (Nov. 1, 2004).
10. (Invited) *N. Nuntawong, S. Birudavolu,* C.P. Hains, *S. Huang*, H. Xu and D.L. Huffaker, "Quantum dot lasers based on a stacked and strain-compensated active region grown by metal-organic chemical vapor deposition," Virtual Journal of Nanoscale Science & Technology (May 16, 2005).
11. D.L. Huffaker, P.K. Bhattacharya, Source: Proceedings of SPIE - The International Society for Optical Engineering, v 5734, Quantum Dots, Nanoparticles, and Nanoclusters II, 2005, 164p (2005).
12. (Invited) *N. Nuntawong, S. Huang*, Y.-B. Jiang, C.P. Hains and D.L. Huffaker, "Defect dissolution in strain-compensated, stacked InAs/GaAs quantum dots grown by metalorganic chemical vapor deposition," Virtual Journal of Nanoscale Science & Technology (September 19, 2005).
13. *N. Nuntawong, P.S. Wong, Y. C. Xin, C. P. Hains, S. Huang*, L. F. Lester and D.L. Huffaker, "Strain-compensation in closely-stacked quantum dot active regions grown by metal organic chemical vapor deposition" SPIE Proceedings – Photonics West 2006.

14. *D.L. Huffaker, C.*P. Hains, *N. Nuntawong Y. C. Xin, P. S. Wong*, L. Yan, S. R. J. Brueck and L. Lester "Temperature-dependent photoluminescence from patterned InAs quantum dots formed using metalorganic chemical vapor epitaxy," Virtual Journal of Nanoscale Science & Technology, February 13, 2006.

Conference presentations

1. **(Invited) D.L. Huffaker**, "Progress in MOCVD-grown Quantum Dot Lasers," CLEO/PR2003, Taipei, Taiwan, December 18, 2003.
2. **(Invited)** D.L. Huffaker, "Characterization of Atomic Structure in Self-assembled Quantum Structures", Physics of Quantum Electronics Workshop, Snowbird, UT, January 4-8, 2004.
3. **(Invited) Diana Huffaker,** "Patterned Quantum Dot Formation", Frontiers of Optics Symposia, Estes Park, CO, Aug. 9-12 2004.
4. *S.Birudavolu*, S.Q. Luong, C.P. Hains and **D.L. Huffaker,** "Selective Area Growth using In-situ Mask Removal" LEOS Annual Meeting, San Juan, Puerto Rico Nov. 11-14, 2004.
5. **(Invited) Diana Huffaker,** "QD formation using strain-based processes and nanopatterning" SPIE Annual, Philadelphia, PA, Oct 22-25, 2004.
6. *S.Birudavolu, N.Nuntawong, S.Huang,* S.C.Lee, S.R.J. Brueck, C.P. Hains and **D.L. Huffaker** "Nano-patterned InAs Quantum Dots Formed using MOCVD" Photonics West, San Jose, CA, Jan. 21-24 2005.
7. **(Invited and fully subsidized) Diana Huffaker**, "Semiconductor Nanostructures", Indian-American Frontiers of Science Symposium, Bangalore, India, January 10-14, 200
8. *N. Nuntawong, Y.C.Xin, P.S. Wong, S. Huang, C.P. Hains*, L. F. Lester and **D.L. Huffaker** "Strain-compensated quantum dot lasers grown by MOCVD", ACCG16/OMVPE12 July 13, 2005.
9. *N. Nuntawong, P.S. Wong, Y. C. Xin, C. P. Hains, S. Huang*, L. F. Lester and D.L. **Huffaker**, "Strain-compensation in closely-stacked quantum dot active regions grown by metal organic chemical vapor deposition" Photonics West 2006, San Jose, CA, January 23, 2006.
10. *J. Tatebayashi, N. Nuntawong, Y. C. Xin, P. S. Wong, S. Huang, C. P. Hains,* L. F. Lester and **D. L. Huffaker**, "Low Threshold Current Injection Lasers based on highly uniform and stacked active regions with strain compensation", IPRM, Princeton, NJ, 5/2006.

Patent Disclosures:

1. D.L. Huffaker, Sandilya Birudovalu, "In-Situ Mask Removal Processing of AlxOy Material in Metalorganic Chemical Vapor Deposition" disclosure submitted, 12/15/04, patent application filed on 1/6/06 # 11/326, 433
2. D.L. Huffaker, Noppadon Nuntawong, "Densely-packed, strain-decoupled quantum dot layers" – converted to full utility application 7/10/06.
3.

b.) Choquette

Publications:

Y. K. Kim, A. J. Danner, J. J. Raftery, Jr., and K. D. Choquette, "Focused Ion Beam Nano-Patterning for Optoelectronic Device Fabrication" IEEE J. Sel. Topics in Quan. Elect. **11**, 1292-1298 (2005).

A. J. Danner, J. J. Raftery, Jr., T. Kim, P. O. Leisher, A. V. Giannopoulos, and K. D. Choquette, "Progress in Photonic Crystal Vertical Cavity Lasers," (invited) IEICE Trans. Electron. **E88**, 944-950 (2005).

Conference presentations

Y. K. Kim, V. C. Elarde, J. J. Coleman, and K. D. Choquette., "Electrically Injected Photonic Crystal Light Emitters with Spatially Localized Gain" 2006 Lasers and Electro Optics Meeting, Montreal, Canada (Oct. 2006).

Y. K. Kim, E. W. Young, and K. D. Choquette, "Small Pitch Vertical Cavity Surface Emitting Laser Arrays" 2004 Conference of Lasers and Electro Optics, San Francisco, CA (May 2004).

Patent Disclosures: